Semnan University

Mechanics of Advanced Composite Structures

Journal homepage: https://macs.semnan.ac.ir/

ISSN: 2423-7043

Research Article

Experimental Evaluation of Low-Velocity Impact Performance of Glass–Basalt Hybrid Composites: Influence of Fiber Weight Fraction and Impact Energy Levels

Chandreshkumar Jayantilal Vyas*, **Ramdevsinh Lalubha Jhala**

Department of Mechanical Engineering, Marwadi University, Rajkot 360003, Gujarat, India

ARTICLE INFO

Article history:

Received:
Revised:
Accepted:

Keywords:

Glass fiber;
Basalt reinforcement;
Hybrid composite;
Weight fraction;
Impact energy;

ABSTRACT

The growing demand for lightweight structural materials with high impact resistance and energy absorption has driven research into hybrid composites. This study aims to develop a hybrid composite by combining natural basalt fiber with synthetic glass fiber and evaluating the effect of basalt fiber weight fraction on low-velocity impact performance. Composite laminates were fabricated using the hand lay-up technique with epoxy as the thermosetting matrix and reinforced with glass and basalt fibers at varying basalt contents: 0%, 18%, 36%, 52%, 72%, and 100%. Low-velocity impact tests were carried out as per the ASTM D7136 guidelines at three distinct energy levels: 20 J, 40 J, and 80 J. Internal damage was assessed using visual inspection and C-scan imaging, while ANOVA was used to statistically analyze the influence of fiber weight fraction on impact force, energy absorption, and damage area. Pure basalt laminates demonstrated high stiffness but brittle failure, while pure glass laminates absorbed more energy due to their higher ductility. The results revealed that among the hybrid laminates, the laminate with 52% basalt fiber demonstrated the most balanced combination of stiffness, energy absorption, and damage area, exhibiting strong hybrid synergy across all energy levels. These findings demonstrate the potential of basalt-glass hybrid composites as sustainable, lightweight, and impact-resistant materials.

1. Introduction

Polymer matrix composites, because of their superior specific strength and stiffness over metal, are extensively used in various industries, including aerospace, automotive, renewable energy systems, marine, sports, and medical devices, as well as the construction and space industries [1–4].

To enhance the composite material properties, a hybrid composite is developed by combining two or more dissimilar fibers with a matrix at the macroscopic level. Hybrid composites can minimize the disadvantages of several fiber types while combining their benefits. This allows materials to be customized to meet certain demands [5, 6]. Although synthetic fibers like carbon, glass, and Kevlar have long been utilized in polymer matrix composites to create lightweight

* **Corresponding author.**
E-mail address: *chandreshkumar.vyas@marwadieducation.edu.in*

Cite this article as:

https:

materials with desirable qualities, their adverse impact on the environment has generated interest in more environmentally friendly substitutes. Recent research indicates that natural fibers such as jute, flax, kenaf, bamboo, sisal, and others are growing more popular due to their availability, affordability, and good mechanical properties [7, 8]. The impact resistance and penetrating behaviour of these hybrids have been the subject of investigations aimed at enhancing their suitability for existing structural applications [9].

Basalt, a kind of volcanic rock, is created when lava rapidly cools near the Earth's surface. It comprises most of the crustal rocks on Earth [10]. Basalt performs extremely well at high temperatures and does not shrink, in contrast to glass fiber [11]. Basalt fiber (BF), due to its unique characteristics and eco-friendliness, is becoming more and more popular as a material for sustainable development. Derived from vast renewable resources, basalt is non-toxic, non-flammable, and resilient to explosions. It leaves less of a footprint on the environment than carbon or glass fibers [12].

Givanni and Belingardi examined the impact behaviour of UD and woven glass-fiber-epoxy composite laminate plates through drop-dart tests. Kinematic analysis was carried out using the integration of force-time data from the impact response. To investigate the impact response parameters, such as impact energy, damage degree, first damage force, and maximum force, were used [13]. R.A. Brooks et al. [14] studied low velocity impact on quasi-isotropic carbon fiber epoxy laminates for energy from 2J to 15J on different thickness plates. Various damages, such as matrix cracking, fiber debonding, and interlaminar delamination, were observed in this research work. Raluca Maier et al. [15] performed a low-velocity drop weight impact test of 33J on various glass-carbon fiber hybrid composites to determine their ability to sustain loads during low-speed impact events. They have observed that there was no significant difference in peak loads for the same impact energy; however, the initiation threshold changed significantly along with the damage area. The impact energy-absorbing capability of clean epoxy and bamboo composites, as well as bamboo/glass hybrid composites, was studied by Ain Umaira Md Shah et al. [16]. Sandwich-structured hybrids were produced by embedding woven glass fiber into epoxy composites filled with bamboo powder. The impact resistance of the composites was greatly increased by the addition of woven glass fibers. There was an investigation into the impact response of glass and carbon fiber laminate composites by Hafiz et al. [17]. Drop weight tests indicate that hybrid laminate displays superior performance compared to laminates made of carbon or glass fibers alone, as evidenced by their higher maximum load capacity and lower maximum deflection. Thus, properly designed hybrid composites can significantly enhance the impact resistance of composites [18].

Mustafa Albayrak et al. assessed the low-velocity impact behaviour of a curved sandwich composite made up of woven glass fiber and ethylene propylene diene monomer rubber. It was observed that using EPDM rubber as an inner layer helps to improve energy absorption of the composite, and as an outer layer helps to reduce damage [19]. Non-destructive testing (NDT) techniques were used to assess the delamination properties of CFRP laminates during low-velocity impact tests [20, 21]. The ultrasonic phased-array NDT evaluated characteristics including area, shape, and trend fluctuations to give quantitative insights into delamination damage in addition to visual examination [22].

Y. Shi et al. [23] used computational and experimental methods to investigate the impact behaviour of carbon fiber metal laminates (FMLs). X-ray computed tomography (X-RCT) and ultrasonic C-scanning were used to evaluate damage at low impact energy (≤30 J). For force and absorbed energy, numerical projections closely matched experimental data, successfully resembling delamination as verified by non-destructive methods. In the experimental research work on low-velocity impact behaviour in hybrid composites made with Kevlar and glass fabrics within a thermoset polyurethane matrix [24], it was observed that hybridization results in enhanced composite performance. The failure mechanisms observed differ from those in traditional epoxy composites, revealing a distinct hybridization effect.

In an experimental study of the low-velocity impact behaviour and damage characteristics of unidirectional, woven fabric, and hybrid unidirectional/woven fabric carbon fiber-reinforced epoxy-based matrix polymer (FRP) laminates [25], post-impact damage was assessed through visual examination and NDT such as ultrasonic phased-array assessment and micro-computed tomography (CT). It was observed that the fiber architecture had a major impact on the laminate's LVI response. Ultrasonic scans were used to evaluate interior damage morphology, and

surface measurements were used to quantify surface damage in an experimental investigation of carbon fiber polymer matrix laminates subjected to LVI with various energy levels [26]. The findings explained that the damage progressed from back surface splitting to delamination and finally to fiber compressive failure.

In recent studies, the performance of sustainable hybrid composites that combine natural and synthetic fibers to enhance mechanical, thermal, and tribological qualities has been investigated. Supian et al. [27] presented a comprehensive review of such materials, highlighting how hybridization strategies involving fibers like kenaf, jute, and bamboo with synthetic reinforcements enhance strength, stiffness, and wear resistance. Raja et al. [28] examined bamboo–glass composites modified with nanoparticles and reported substantial increases in thermal stability and fatigue life. Oliveira et al. [29] examined interlaminar bamboo–synthetic fiber hybrids and found notable synergy in thermal and mechanical behaviour compared to single-fiber systems. Additionally, Salman et al. [30] and Nadzri et al. [31] studied kenaf/glass hybrid composites, focusing on their mechanical properties and low-velocity impact performance. They highlighted how fiber content and orientation affect the overall performance of the composites. The sandwich-type structure made using glass, sisal, and chitosan fibers also showed excellent impact and flexural behaviour for bio-structural applications [32]. These works reinforce the potential of fiber hybridization to achieve a balance between strength, energy absorption, and sustainability—supporting the motivation for the present investigation into glass-basalt hybrid systems.

Although extensive research has been conducted on hybrid composites incorporating glass, carbon, and Kevlar fibers, limited attention has been given to glass–basalt hybrids, particularly with systematic variation in basalt fiber weight fraction. Moreover, the behaviour of these hybrids under different impact energy levels—and the correlation of their performance with C-scan imaging and ANOVA analysis remains underexplored.

This study addresses these gaps by systematically examining the influence of the basalt fiber weight fraction on low-velocity-impact performance at multiple energy levels. Key parameters such as stiffness, energy absorption, and damage characteristics were analysed, and the hybrid effect was assessed using the Rule of Mixtures. This research will support the development of lightweight, sustainable, and impact-resistant composites with basalt fiber weight fraction serving as a critical design parameter.

2. Materials and Methods

2.1. Materials of Composite Laminate

This research work utilized CT EWR/400 glass fabric and CTB1-FBD-380P basalt fabric. The properties of glass and basalt fiber are given in Table 1. The resin system was supplied by The Bhor Chemicals and Plastics Pvt. Ltd., consisting of low-viscosity colorless bisphenol-A-based liquid epoxy resin and transparent hardener. The properties of resin used in this study are provided in Table 2.

2.2. Configuration of Laminates

As seen in Table 3, a total of six laminates were created utilizing the hand layup method. Epoxy and hardener were combined in a 100:35 weight ratio. To eliminate air bubbles from the resin, the resin was stirred for around ten minutes. The resin was applied to the fabric during preparation of the laminates using a 2-inch nylon hairbrush, followed by using a bubble paddle roller to release any trapped air between the layers of fibers. To ensure uniform quality and minimize void formation, a bubble paddle roller was thoroughly used during each layer placement. Additionally, a uniform weight was applied on top of the laminate to remove excess resin and promote compaction. The laminate was allowed to cure in the mould for 24 hours, after which the applied weight was removed, and the laminate was demoulded.

Table 1. Fiber properties provided by the manufacturer

Material	Cured Density (g/cc)	Tensile strength (MPa)	Tensile modulus (GPa)	Elongation at break (%)	Layer thickness (mm)	Aerial Weight (g/m^2)	Weave style	Warp (0^0) and Weft (0^0)
Glass Fiber	2.55	3.4	72	4.70	0.4	400±8%	Plain BD	Woven Roving 12K
Basalt Fiber	2.80	4.8	89	3.15	0.38	380±5%		

Table 2. Resin properties provided by the manufacturer

Material	Cured Density (g/cc)	Tensile strength (MPa)	Tensile modulus (GPa)	Ultimate elongation (%)	Viscosity at 25^0 (cP)	Cure time at 25^0C (hours)
Resin	1.2	60	2.5	3.5	850	24

Table 3. Different Laminate Configurations

Configuration Name	Glass Basalt Layer ratio	Stacking sequence	Type of ply	Thickness (mm)
LS1	G11:B0	G G G G G G G G G G G	Plain	4.53
LS2	G9:B2	B G G G G G G G G G B	Hybrid	4.47
LS3	G7:B4	B B G G G G G G G B B	Hybrid	4.38
LS4	G5:B6	B B B G G G G G B B B	Hybrid	4.31
LS5	G3:B8	B B B B G G G B B B B	Hybrid	4.26
LS6	G0:B11	B B B B B B B B B B B	Plain	4.22

The overall thickness of the laminate decreases as the number of basalt fiber layers increases. This trend was expected, as the basalt fiber layer thickness is 0.38 mm, while the glass fiber layer thickness is 0.40 mm. A relatively small variation is observed in the overall thickness of the different laminate configurations. From the fabricated laminates, specimens were cut as per the ASTM standard using the abrasive water jet cutting technique.

3. Testing of Composites

To investigate the effect of different basalt fiber content on the performance of glass-basalt hybrid composites, various tests, such as density, fiber weight fraction, and low velocity impact (LVI), were conducted according to ASTM standards. For each configuration and each impact energy level, three specimens were tested to confirm the repeatability of the experimental test data, and the average value of the data is presented. The consistency across these specimens was confirmed by the low standard deviations observed in the measured parameters. This approach ensured statistical reliability and minimized experimental variability.

3.1. Density and Weight Fraction

A specimen was subjected to a density test in accordance with ASTM D792 criteria. Using a density balance unit instrument, the specimen's weight was determined in both water and air, and its density was assessed [33].

The weight fraction of fiber and resin in the cured composite is ascertained by an ignition loss test performed in accordance with ASTM D2584 [33]. For two and a half hours, the specimen was heated in a muffle furnace to 575 ^{0}C. After that, the specimen was left to cool for an hour at room temperature. The weight of the matrix lost during ignition was measured, and the weight fractions of the aggregate and individual fibers were calculated and published here.

3.2. Low-Velocity Impact Test

Low-velocity impact experiments were performed on a drop-weight test machine shown in Fig. 1, as per ASTM D7136 standard. The impactor has a hemispherical nose with a diameter of 16 mm and a mass of 9.835 kg. The impact energy was adjusted to 20 J, 40 J, and 80 J by altering the height of the impactor to 0.21 meters, 0.42 meters, and 0.83 meters, respectively.

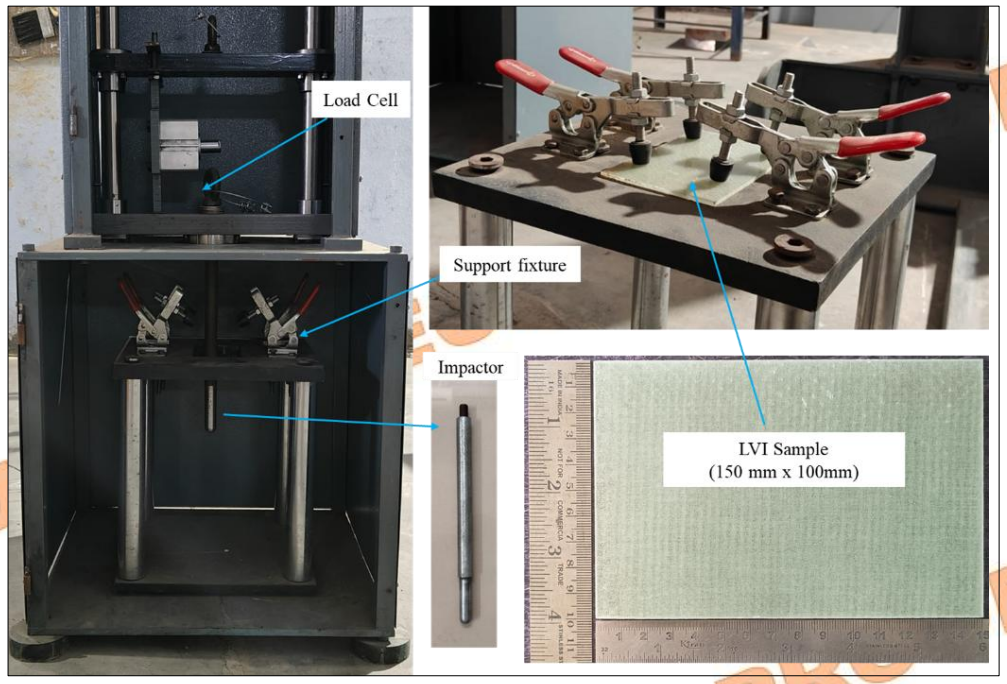

Fig. 1. Experimental setup for low-velocity impact testing used in this study

The drop height was determined by the equation of potential energy,

$$E = mgh \quad (1)$$

where E = energy of impact, m = impactor mass, g = gravitational acceleration, and h = height of drop

Composite laminate samples with dimensions 150 mm x 100 mm x 't' mm were used for the impact experiments. The sample rate of data collected here is 50 kHz. The load cell measured the force versus time data. After getting these data, the important parameters, which include velocity, deformation, and absorbed energy, were calculated using low-velocity impact test equations [34]. Numerical integration was carried out using the trapezoidal rule and a MATLAB algorithm. To know the statistical importance of fiber weight fraction on LVI test parameters, statistical analysis in this research was conducted for each composite laminate's impact force, absorbed energy, and damaged area at different energy levels using a one-way analysis of variance (ANOVA) test at a 5% level of significance (95% confidence level). To ascertain if the null hypothesis can be rejected, we compare the p-value and alpha value. If the p-value is smaller than the alpha value (0.05), the data are considered significant [35].

4. Results and Discussion

This section gives the results from the low-velocity impact test, ignition loss test, and density test. Density was measured by Archimedes' principle, while the matrix digestion method was used to calculate the fiber fraction. Here, statistics in the graphs are the means of experimental results, while vertical bars represent the standard deviations.

4.1. Density and Weight Fraction

Table 4 displays the weight fraction and density of various laminates. The total fiber fraction is consistent across laminates (ranging from 61% to 64%). Because all the laminates were made by hand, it was difficult to maintain the matrix distribution and roller pressure the same while the laminates were being made, and small changes in the overall fiber fraction were seen. In the laminates from LS1 to LS3, the density goes up a little because the higher fiber fractions and the higher density of the basalt work together. As the basalt content rises above LS3, the density drops in LS4. This is because the lower GSM of basalt fiber (380 gsm) compared to glass fiber (400 gsm) starts

Table 4. Weight Fraction of fibers and Density of laminates

Laminate	Weight fraction of Glass fiber (%)	Weight fraction of Basalt fiber (%)	Total Fiber Fraction in laminate (%)	Density (gram/cm^3)
LS1	100	0	61	1.7588
LS2	82	18	62	1.7602
LS3	64	36	64	1.7753
LS4	48	52	63	1.7302
LS5	28	72	64	1.7337
LS6	0	100	62	1.7230

to have a bigger effect, causing the laminate density to drop, even though basalt fibers have a higher intrinsic density. The LS5 laminate shows a minor increase in density, as the fiber fraction is a little higher than that of the LS4. Lower GSM indicates a thinner material that has a low aerial density and fewer fibers per unit area. This is why the non-hybrid laminate LS1, which solely consists of glass fiber, exhibits a higher density compared to the non-hybrid laminate LS6, which solely consists of basalt fiber.

4.2. Low-Velocity Impact Test Results

The work of this study has been based on impact tests conducted on materials at three different levels, all aiming to establish their response in relation to force, energy absorbed, and the damage area. The 20 J impact falls into the low-energy range, making it ideal for testing the material under less severe conditions and for detecting minor surface damage or the initial delamination in composite materials. The 40 J impact, considered a moderate-energy impact, was used to track the accumulation of damage over time. The 80 J impact would be relevant to high-energy impacts that correlate with the strength and integrity of a material against gross failures, such as delamination, cracks, or penetration. Analysis of the LVI test results is discussed in the following section.

4.2.1. Effect of Hybridization on Impact Force

The impactor applies the impact force on the material during the collision. These forces are generally seen to rapidly increase as the impactor contacts the surface, reach a peak, and begin to decrease as the material absorbs the energy or undergoes deformation. The peak impact force is an important reference, as it indicates the maximum force that the material undergoes before any possible damage, cracking, or failure.

FigureFig. *2*(a) indicates that at 20 J, the energy impact is relatively low for all configurations, and the materials exhibit a mostly elastic response. All composite laminates seem to handle the energy well without significant differences in performance and exhibit similar behavior with minimal deviation from each other, which can be seen by close clustering for the force-time curve. The force versus time curves display a symmetric profile with gradual falling phases, indicating minimal plastic deformation. In the 20 J impact as shown in Fig. 2(b), the maximum impact force for the LS6 laminate (100% basalt) was 6177.38 N, which is slightly higher than that of the LS1 laminate (100% glass), which recorded 6115.61 N. At 20 J, the higher contact force in LS6 is due to the greater stiffness of basalt fiber. As basalt fiber content increases from 0% (LS1) to 36% (LS3), the maximum contact force decreases, likely due to reductions in overall stiffness and mismatches in material properties that result in stress concentration at the interface of glass and basalt fiber [36]. Laminate LS4 (52% basalt) exhibits a marginal improvement in the maximum contact force because of what appears to be a fine balance between stiffness and flexibility. However, for laminate LS5 (72% basalt), the peak force slightly drops again, likely due to a loss of hybrid synergy—where increased brittleness and fiber-matrix mismatch limit the laminate's ability to sustain and transfer impact loads effectively. At a low-energy impact, the load transfer across thickness is not very effective, leading to uneven load distribution between the glass and basalt fiber layers [37].

At 40 J, Fig. 3(a) shows similar behaviors to what was seen at 20 J, but with more oscillation and impact force because the 40 J impact has more.

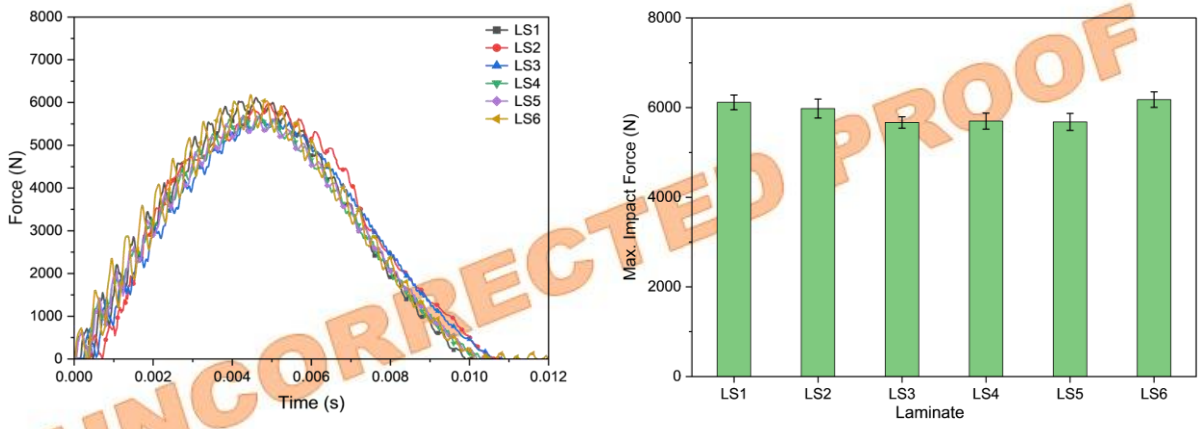

Fig. 2. Impact force response of different laminates subjected to 20 J impact energy: (a) Force–time response curves for various laminates, (b) Comparison of maximum impact force observed for each laminate configuration

energy. As shown in Fig. 3(b), at 40 J, non-hybrid basalt fiber laminate LS6 also shows a maximum impact force of 9060.56 N, which is higher than that of non-hybrid glass fiber laminate LS1, which recorded 8567.02 N. The addition of basalt reduces the maximum force in laminate LS2 (18% basalt). This implies a transitional step whereby the characteristics of the fibers do not match, and the stress waves do not transmit appropriately [38], thus making the hybrid composite inefficient at this fiber ratio at 40 J. An increase in hybrid effects may explain the force recovery recorded in LS3 (36% basalt). Among all hybrid composites, LS4 (52% basalt) exhibits the highest maximum impact force at 8916.14 N, indicating an ideal balance between stiffness and toughness. In comparison with the regular glass fiber composites (LS1), the impact force of basalt-dominant hybrid composites (LS4, LS5) is higher at 40 J.

FigureFig. *4*(a), at 80 J, shows the elevated energy level, all the laminates exhibiting plastic-like behaviour, and it creates distinct variations in their performance. When the impactor strikes a laminate, there are stress waves traveling through it that reflect from the fiber matrix interfaces, inducing fluctuations in force [39]. As damage escalates, delamination between layers interferes with load transfer, intensifying oscillations, and fiber breaking and matrix cracking cause abrupt decreases in force [40]. The force response is further affected by variations in contact stiffness brought on by different fiber characteristics (such as glass versus basalt). As shown in Fig. 4(b), at 80 J impact, the basalt fiber laminate (LS6) exhibits a higher maximum impact force of 11309.73 N compared to only the glass fiber laminate (LS1), which shows a force of 9823.88 N. Pure basalt fiber exhibits good stiffness but lacks the toughness needed for high-energy impacts. As basalt is introduced in glass fiber, suboptimal bonding and uneven stress distribution at the glass-basalt interface lead to reduced impact resistance [37] and, consequently, the impact force in laminate LS2 (18% basalt). Increasing basalt content (LS3, LS4, LS5) results in a marked improvement in contact force due to better toughness and hybrid synergy. LS4 (52% basalt) has the greatest maximum impact force of 11834.65 N among all laminates. The performance of non-hybrid basalt (LS6) laminate is marginally inferior to that of hybrid laminate LS5, attributable to the greater brittleness of basalt.

Peak impact force rises for all laminate designs as impact energy increases (20 J → 40 J → 80 J). Higher force levels typically result from increased impact energy, as expected. The peak contact force is in the centre of the curve at 20 J impact; however, the loading period is shorter than the unloading time for 40 J & 80 J energy impact curves when partial penetration or perforation takes place. At 40 J and 80 J energy impacts, the perforation causes an increase in oscillations in the curve. These differences can be attributed to the mismatch in stiffness between glass and basalt fibers, which affects stress transfer at the interface. Poor interfacial bonding or stiffness mismatch can cause stress concentration and early microcracking. In

hybrid laminates, especially at lower basalt content, ineffective load transfer between glass and basalt layers may reduce the overall contact force. As basalt content increases and becomes dominant, the stiffer nature of basalt improves contact force, although at the cost of reduced ductility.

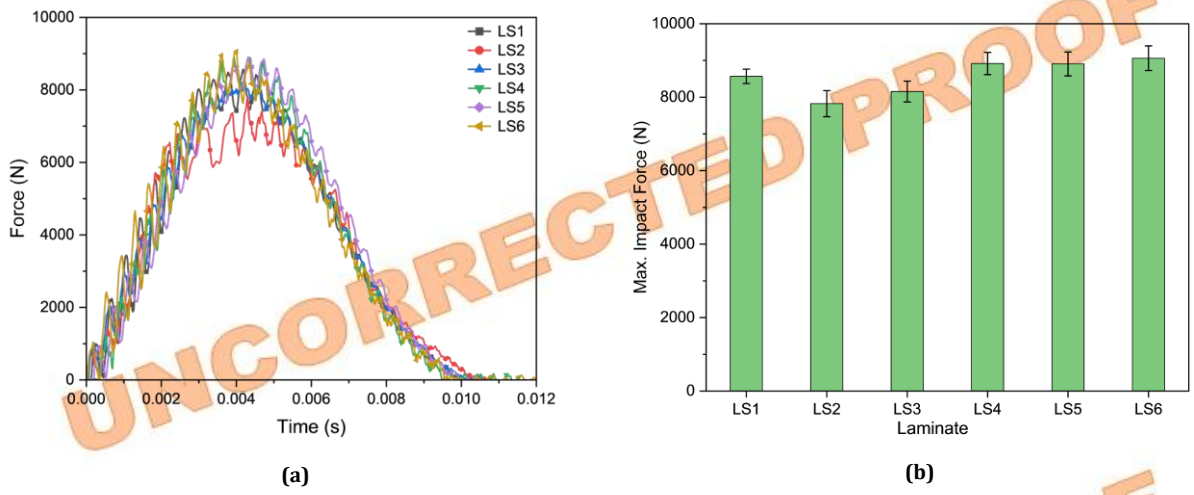

(a) (b)

Fig. 3. Impact force response of different laminates subjected to 40 J impact energy: (a) Force–time response curves for various laminates, (b) Comparison of maximum impact force observed for each laminate configuration

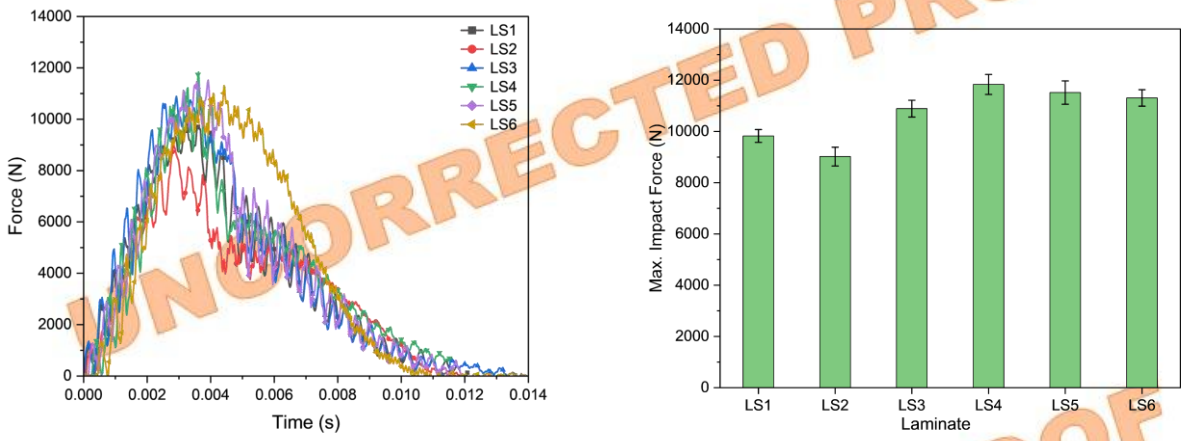

(a) (b)

Fig. 4. Impact force response of different laminates subjected to 80 J impact energy: (a) Force–time response curves for various laminates, (b) Comparison of maximum impact force observed for each laminate configuration

4.2.2. Effect of Hybridization on Absorbed Energy

The force vs. deformation curve is important for low-velocity impact analysis of composites because the area under this curve gives insight into energy absorption. The curve reveals the elastic and plastic deformation phases, showing how the composite stores and absorbs energy. Sharp changes in the curve often correlate with damage events like matrix cracking, delamination, or fiber breakage.

FigureFig. *5*(a) shows that for a 20 J impact, LS6 exhibits a steeper initial slope, indicating higher stiffness and rigidity. In contrast, LS1 shows a gentler slope, representing lower stiffness and greater flexibility. Compared to plain laminates (LS1 and LS6), all the hybrid laminate curves shift toward the right side, which represents an increase in flexibility. In the initial phase, materials experience elastic deformation, where the structure absorbs energy without permanent deformation. After the peak, materials start dissipating energy through frictional damping—

where crack faces rub against each other—and plastic deformation, which involves localized yielding near crack tips or deformation zones [41]. The hybrid laminate LS2 absorbs less energy than the non-hybrid laminate LS1. This suggests that this composition is less effective and doesn't provide a balance between glass and basalt at 20J.

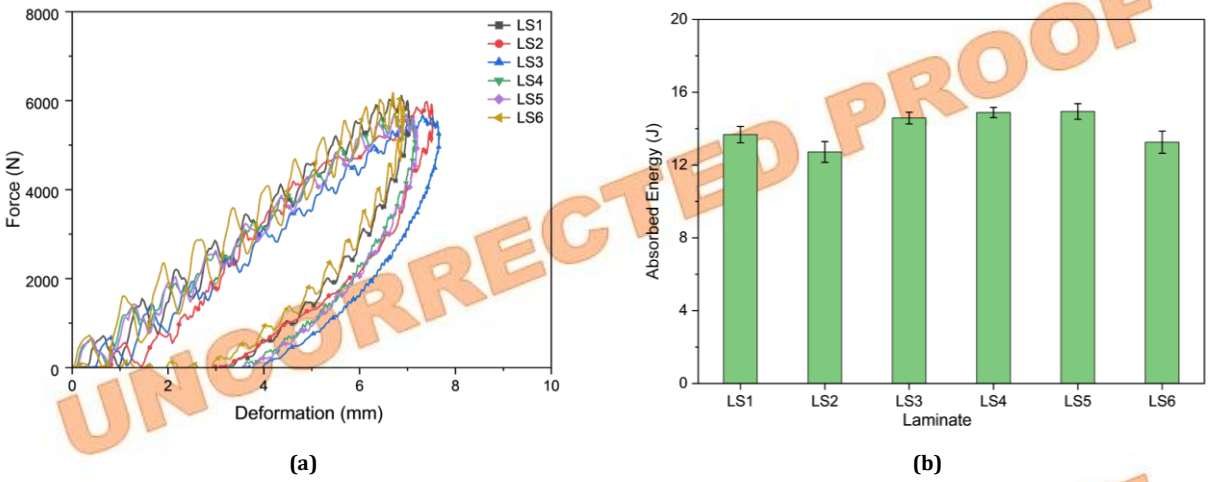

(a) **(b)**

Fig. 5. Impact response of different laminates subjected to 20 J energy impact: (a) Force–deformation curves for various laminates, (b) Comparison of maximum energy absorbed by each laminate configuration

As shown in Fig. 5(b), hybrid laminates LS3 to LS5 show higher energy absorption compared to plain glass fiber laminate (LS1) and plain basalt fiber laminate (LS6). Hybrid Laminate LS5 exhibits the highest energy absorption of 14.94 J. Non-hybrid laminate LS1 and LS6 show energy absorbed of 13.67 J and 13.26 J, respectively. Slightly higher energy absorption in glass fiber laminate LS1 indicates better plastic deformation and progressive energy dissipation. The basalt fiber laminate (LS6) shows slightly lower energy absorption, indicating brittle behaviour and limited plastic deformation [42].

As shown in Fig. 6(a), the force–deformation curves for all laminates at 40 J impact exhibit a trend like that observed at 20 J impact. For all hybrid laminates from LS2 to LS5, the deformation is higher than in LS1. Basalt has higher stiffness and strength than glass, but glass has higher elongation at break. This mismatch in properties reduces the overall stiffness of hybrid laminates, allowing more deformation at 40 J impact. LS1 and LS2 lose energy faster, as indicated by the steeper fall after the peak. This indicates that the damping and energy dissipation are higher in the laminates dominated by glass fibers. The addition of basalt reduces the energy absorbed marginally in the instance of laminate LS2 compared to LS1. The hybrid laminate LS4 exhibits a maximum absorption of 30.46 J of energy when compared to other laminates. Non-hybrid laminate LS1 and LS6 absorb energy of 30.28 J and 29.60 J, respectively, as shown in Fig. 6(b).

As shown in Fig. 7(a), at high energy impact (80 J), as the impact progresses, failure, such as cracks, fiber pull-outs, and delamination, converts kinetic energy into heat and internal structural damage. This reduces vibration energy, causing oscillations to reduce. Laminate LS1 absorbs the most energy of 78.30 J. Laminate LS6 absorbs the least energy of 70.11 J. The hybrid laminate LS4 exhibits a maximum absorption of 76.15 J of energy when compared to other hybrid laminates.

From Fig. 7(b), higher basalt content (LS5, LS6) laminate energy absorption was reduced, as the material does not deform enough to absorb impact energy efficiently. Lower basalt content (LS1, LS2) enhances damping properties from glass fiber, allowing more energy absorption. In Laminate LS4 (52% basalt), the most favourable balance between stiffness and damping resulted in the highest energy absorption among all hybrid laminates. This suggests that basalt and glass fiber interact effectively at this ratio, allowing for both impact resistance and energy dissipation. The absorbed energy varies between the laminates based on how the energy was dissipated. Glass fibers, with higher elongation at break, tend to undergo plastic deformation and microcracking, absorbing more energy. In contrast, basalt fibers behave in a more brittle manner, leading to lower energy absorption. The efficiency of energy dissipation also depends on the fiber–matrix interface; better bonding

facilitates progressive damage mechanisms, while poor bonding can lead to sudden delamination and lower energy absorption.

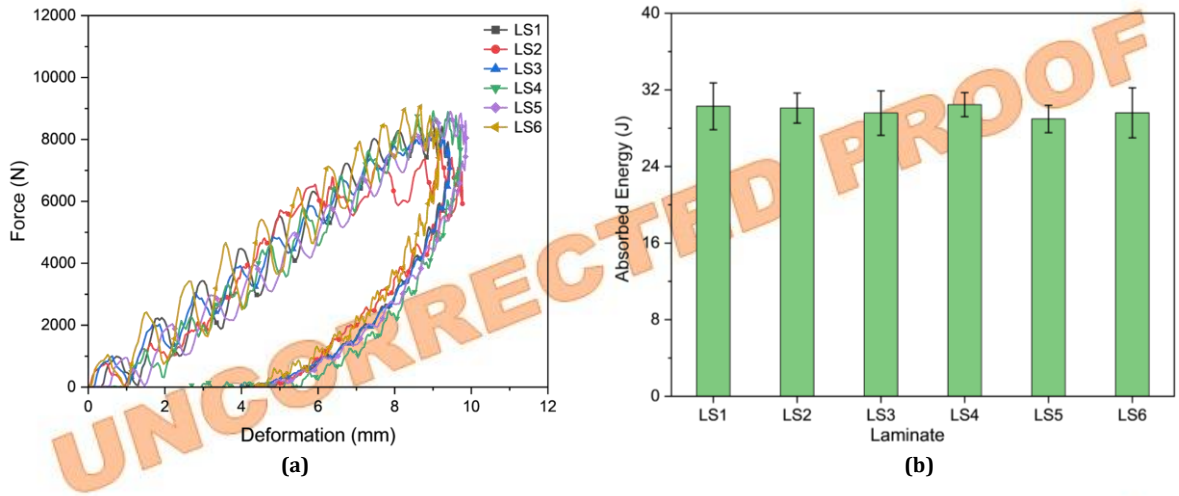

Fig. 6. Impact response of different laminates subjected to 40 J energy impact: (a) Force–deformation curves for various laminates, (b) Comparison of maximum energy absorbed by each laminate configuration

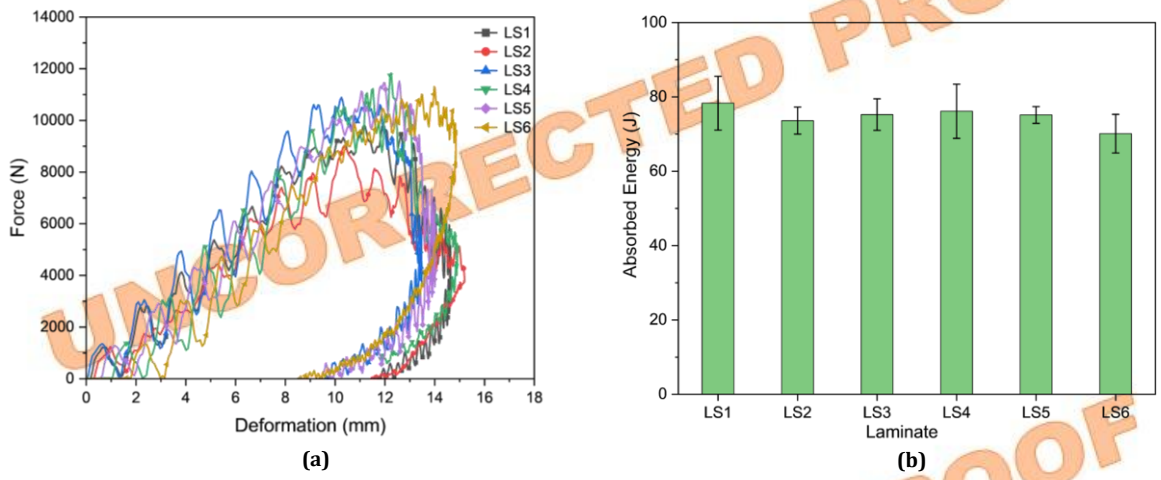

Fig. 7. Impact response of different laminates subjected to 80 J energy impact: (a) Force–deformation curves for various laminates, (b) Comparison of maximum energy absorbed by each laminate configuration

4.3. Effect of Hybridization on Damage Area

Damage area in low-velocity impact is an important parameter to check structural integrity and long-term performance. It is a measure of material degradation that affects strength, stiffness, and durability. The following section presents an analysis of the damage area resulting from low-velocity impacts on laminates LS1 to LS6 at different energy levels.

From Fig. 8, at 20 J impact, a progressive increase in damage severity from laminates LS1 (100% glass) to LS6 (100% basalt) is observed. The non-impact side of all hybrid laminates shows very little damage compared to the plain laminates LS1 and LS6. Laminate LS1 has a localized indentation and some minor fiber breakage on the non-impact side. The corresponding C-scan shows a circular dark region, confirming subsurface damage and delamination. LS2 (18% basalt) has greater damage, with a greater delaminated area seen in the C-scan compared to LS1. The damage zone expands from LS2 to LS3(36% basalt), with more impact-induced failure. Laminate LS3 and LS4 (52% basalt) exhibit widespread damage in the weave direction, with long delamination features in

their C-scans, which indicate directional energy dissipation. LS5 (72% basalt) has less fiber breakage compared to LS4, but C-scan images indicate significant internal failure due to the matrix

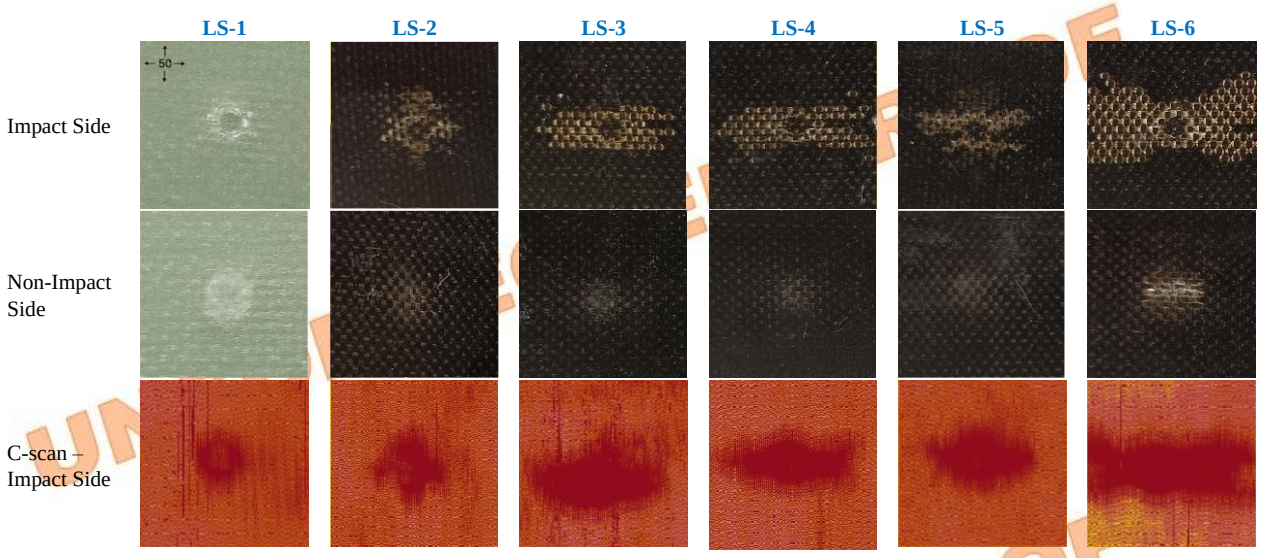

Fig. 8. Visual and C-scan images showing the damage zones in different laminates subjected to a 20 J low-velocity impact.

cracking. LS6 (100% basalt) sustains the maximum damage, the most localized breakage of the fibers, and the largest and most irregularly delaminated region in the C-scan. As shown in Fig. 11, the damage area in laminate LS1 is 138.43 mm^2. The addition of basalt increases the damage area in LS2 and LS3. The damaged area with laminates LS4 and LS5 is a little smaller than it was in LS3. This suggests that energy is being dissipated better, and there is better interaction between the fibers and the matrix, which may help to stop the damage from spreading. LS6 has a maximum damage with a damage area of 564.73 mm^2. This indicates that there is widespread damage in the thickness direction.

From Fig. 9**,** at 40 J impact on the non-impact side, all laminates exhibit a dent. Hybrid laminates LS3, LS4, and LS5 sustain less damage on non-impact sides compared to laminates LS2 and LS6. As the amount of basalt in the sample rises from LS1 to LS6, the damage area grows from 220.23 mm^2 in LS1 to 967.06 mm^2 in LS6, as shown in Fig. 11. In LS1, there was only localized denting, minimal fiber breakage, and minor delamination. The impact-side images in LS6 reveal the highest degree of fiber rupture and matrix failure. The impact side also shows increased delamination, especially in LS5 and LS6, where subsurface cracking spreads beyond the apparent impact zone. LS2 shows higher levels of resin cracking than LS1. The C-scan reveals an elongated delamination pattern with increased internal failure in LS2. Damage area in laminate LS3 has a sharp increase compared to LS2, while LS4 shows a slight decrease in damage area compared to LS3, suggesting a temporary improvement in energy absorption. However, LS5 and LS6 experience further expansion of damage areas compared to LS4, with LS6 showing the most extensive delamination and fiber-matrix failure.

As shown in Fig. 10, perforation at the impact side with a dent at the non-impact side is observed for all the laminates at 80 J impact. LS2 demonstrates a larger damage area profile with larger dents and significant fiber breakage and matrix cracking compared to LS1. In LS2, fiber splitting is visible on the opposite side, and energy dissipation beyond the impact point is indicated by an irregular delamination extending outward, as evidenced by the C-scan. LS4 exhibits considerable reductions in the damage area, characterized by significant damage along the fiber weave pattern and evident indications of fiber breaking and resin delamination on the impact side. The non-impact side in LS3 and LS4 exhibits more pronounced fiber splitting; the C-scan pictures reveal extended delamination areas. The damage area increased further in LS5 and LS6, with LS6 exhibiting the highest levels of matrix failure, delamination, and fiber breakage. The analysis shows minimal

delamination in LS1 but widespread internal damage in LS6, suggesting that higher basalt content leads to brittle failure, the same as 20 J and 40 J impacts.

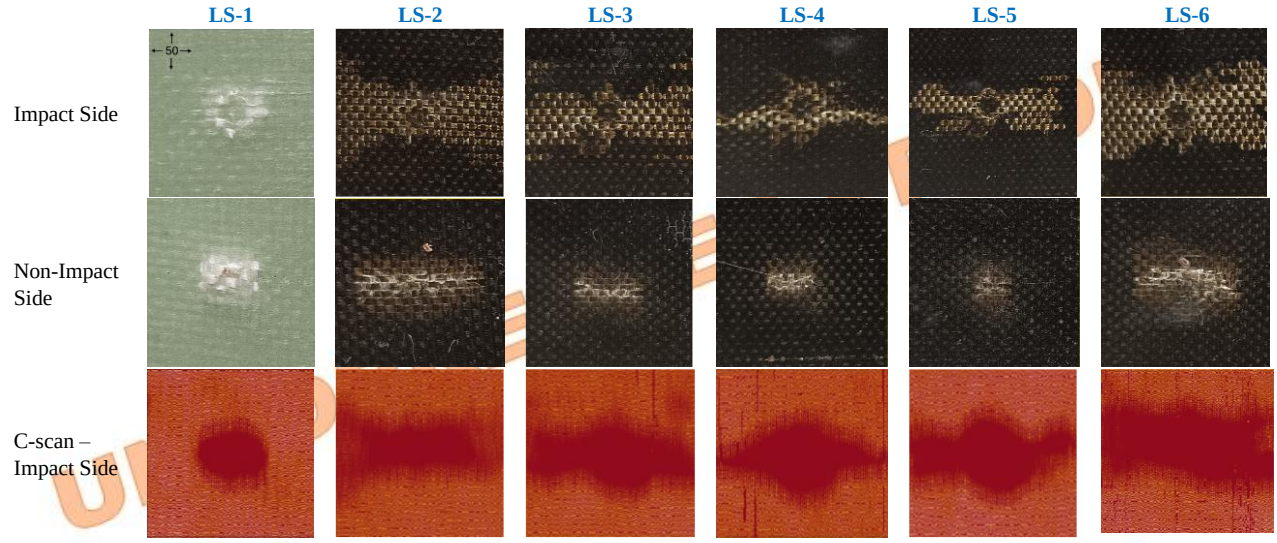

Fig. 9. Visual and C-scan images showing the damage zones in different laminates subjected to a 40 J low-velocity impact

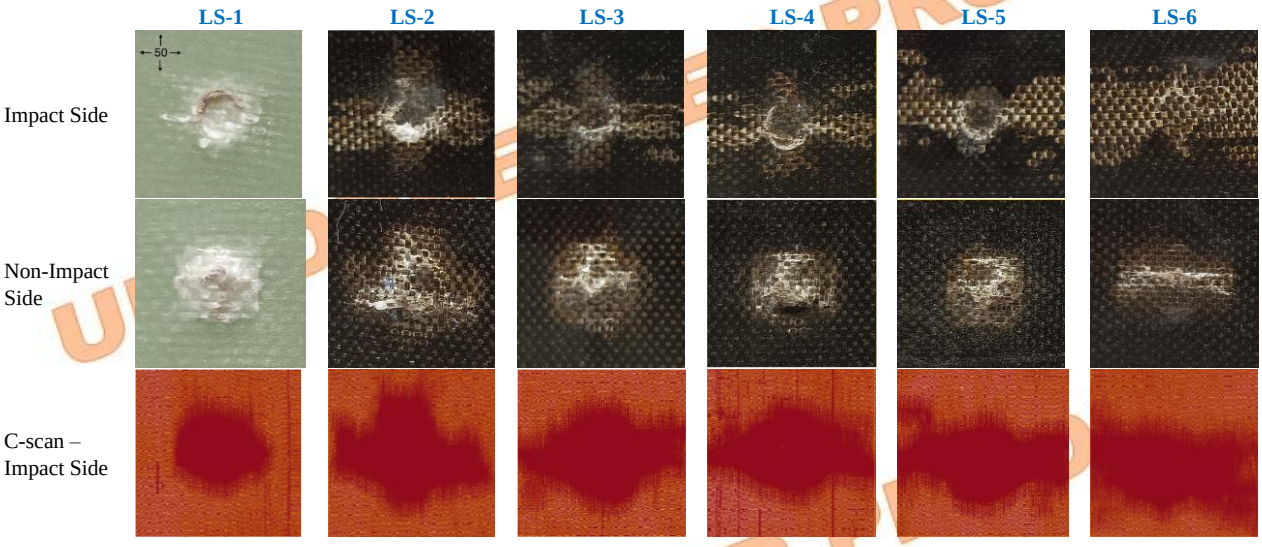

Fig. 10. Visual and C-scan images showing the damage zones in different laminates subjected to an 80 J low-velocity impact

These damage characteristics can be linked to the failure mechanisms and interfacial interactions between the fibers and matrix. Glass fibers, due to their higher elongation at break, can undergo more gradual energy dissipation through microcracking and fiber pull-out, which helps localize damage. In contrast, basalt fibers, being stiffer and more brittle, are prone to sudden cracking and poor strain accommodation, especially under high-energy impacts. When basalt dominates the laminate (e.g., LS6), the poor ductility contributes to larger and more irregular damage zones. Hybrid laminates like LS4 benefit from a synergistic interaction: the glass layers improve toughness and energy dissipation, while the basalt layers contribute stiffness and strength. This synergy helps delay delamination and distribute stress more uniformly, resulting in reduced damage areas compared to pure basalt or glass laminates.

No complete penetration was observed in any laminate for 20 J, 40 J, and 80 J impacts. The C-scan results highlight that internal damage extends far

beyond visible surface defects, reinforcing the importance of non-destructive evaluation techniques for impact assessment.

Glass fiber has higher ductility, allowing for gradual.

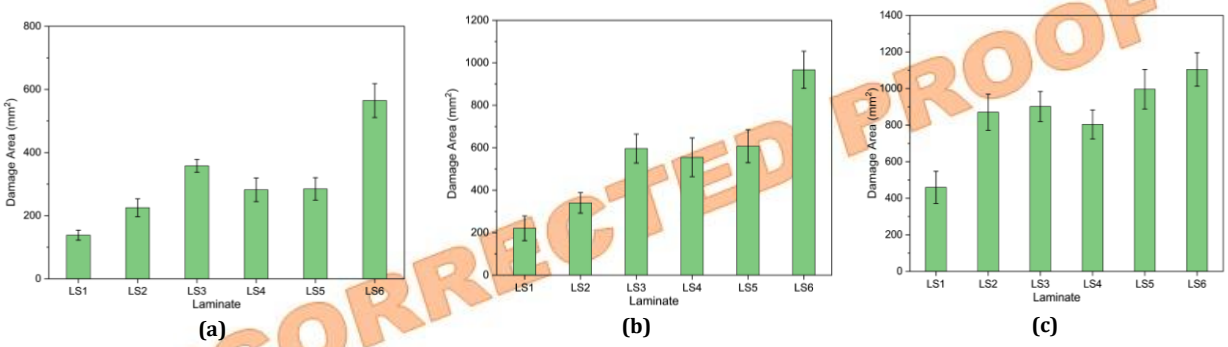

Fig. 11. Comparison of damage areas in various laminate configurations subjected to low-velocity impact at: (a) 20 J impact energy, (b) 40 J impact energy, and (c) 80 J impact energy

energy absorption, and localized damage results in a smaller damage area. The basalt stiffness likely contributes to its brittleness, making it more susceptible to large-scale failure under impact. The images of the impact and non-impact sides further confirm that fiber breakage, resin cracking, and delamination are likely to worsen as basalt content increases.

4.4. Statistical Analysis Using ANOVA

Statistical analysis Table 5 presents the results of a one-way ANOVA statistical analysis of the impact response characteristics of different composite laminates. Weight fractions of basalt fiber in glass-basalt hybrid composite have a significant influence on both the maximum impact force and damage area in low-velocity impact (LVI) tests across all energy levels, as indicated by p-values less than 0.05. The influence of the fiber weight fraction on the maximum impact force increases as the impact energy increases. At 20 J of energy impact, the amount of energy absorbed is statistically significant ($p<0.05$) for the fiber weight fraction. However, this was not observed at higher impact energies ($p>0.05$ at 40 J and 80 J), where energy is sufficient to transfer the load through the material thickness across different fiber layers. At 20 J, the effect of impact energy is relatively small, and energy absorption is dominated by surface and near-surface phenomena like matrix cracking and interfacial debonding. These are highly dependent on fiber form and glass-basalt layer interaction, resulting in statistically significant variation. However, at 40 J and 80 J impacts, more severe, through-thickness damage mechanisms such as delamination and fiber breakage dominate, resulting in more uniform energy distribution across the laminate thickness. Consequently, the influence of fiber weight fraction on energy absorption decreases and is statistically non-significant.

4.5. Hybridization Effect for Energy Absorbed

This study investigates the effect of hybridization by incorporating the Rule of Mixtures using the equations below for the absorbed energy.

$$E_R = E_g W_{fg} + E_b W_{fb} \quad (2)$$

where E_R = Absorbed energy value by rule of mixture, E_g = Energy absorbed by glass fiber laminate (LS1), E_b = Energy absorbed by basalt fiber laminate (LS6), W_{fg} = Weight fraction of glass fiber in laminate, W_{fb} = Weight fraction of basalt fiber in laminate

$$H_e = \frac{E_a}{E_R} - 1 \quad (3)$$

E_a = Absorbed energy value from the impact test.

Positive. H_e indicates a beneficial hybrid effect where the composite performs better than the rule-of-mixtures prediction. Negative. H_e indicates a detrimental hybrid effect, suggesting weaker performance than expected. From Fig. 12 hybrid effects depend on the energy of impact as well as the type of hybrid laminate. LS2 (18% basalt) exhibited a consistently negative hybrid effect at all energy impacts. LS3 (36% basalt) shows a positive hybrid effect only at 20 J impact. LS4 (52% basalt) shows the positive hybrid effect at all impact energies. LS5 (72% basalt) shows a positive hybrid effect at 20 J and 80 J impact. Thus, low basalt

content does not contribute positively, but higher basalt content (≥50%) results in a positive hybrid effect at most of the energy levels.

5. Conclusion

This study examined the low-velocity impact performance of glass–basalt hybrid composite laminates with different weight fractions of basalt.

Table 5. ANOVA results for Impact response parameters of hybrid laminates based on different fiber weight fractions

Impact Energy	Source of Variation	*SS*	*df*	*MS*	*F*	*p-value*
20 J	Maximum Impact Force (N)	812821.96	5	162564.39	5.46	0.008
	Absorbed energy (J)	12.94	5	2.59	12.78	0.000
	Damage Area (mm^2)	185023.62	5	37004.72	27.52	0.000
40 J	Maximum Impact Force (N)	3605658.93	5	721131.79	8.10	0.002
	Absorbed energy (J)	4.63	5	0.93	0.24	0.938
	Damage Area (mm^2)	728175.21	5	145635.04	90.24	0.000
80 J	Maximum Impact Force (N)	17835682.7	5	3567136.5	29.14	0.000
	Absorbed energy (J)	113.15	5	22.63	0.84	0.549
	Damage Area (mm^2)	453714.74	5	90742.95	30.41	0.000

SS-sum of squares; df-degree of freedom; MS-mean square; F value: test statistic; p value: probability of observing the effect due to random chance;

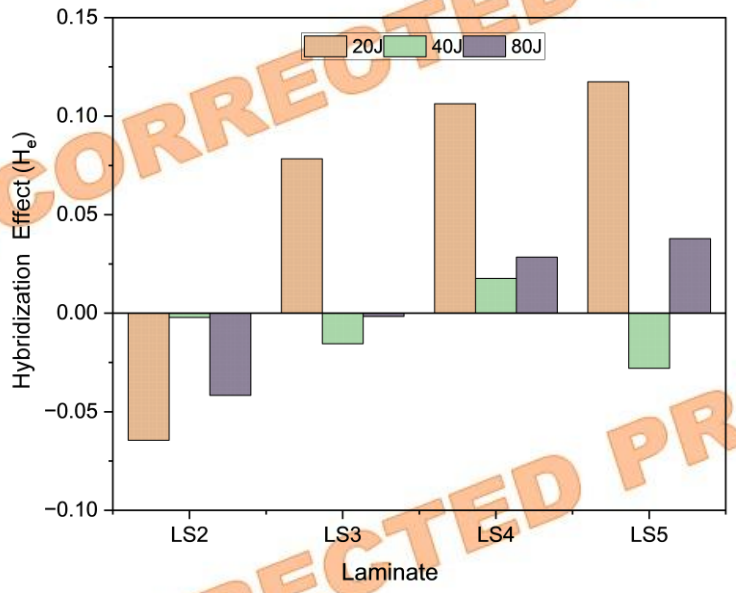

Fig. 12 Variation of hybridization effect across different laminates under impact energies of 20 J, 40 J, and 80 J.

fiber under impact energies of 20 J, 40 J, and 80 J. All laminates can withstand impact energies up to 80 J without complete penetration, demonstrating their structural resilience.

The rigid and brittle nature of pure basalt laminates led to high stiffness and large peak impact forces; however, they suffered from extensive damage areas with limited energy absorption. On the other hand, pure glass laminates consistently absorbed higher amounts of energy while exhibiting lower damage areas owing to their ductility and elongation at break. Hybrid laminates showed a balanced performance and, in some cases, performed better than both pure glass and pure basalt laminates in terms of impact force, energy absorption, and damage area. The laminate

with 52% basalt fiber demonstrates the best balance of higher impact resistance, controlled damage propagation, and energy absorption.

At lower impact energy (20 J), hybrid laminates underperformed in energy absorption compared to glass-dominant ones due to insufficient load transfer across dissimilar fiber layers. At higher energies (40 J and 80 J), however, hybrid configurations performed better due to improved stress distribution and glass-basalt interaction. ANOVA statistical analysis confirmed that the fiber weight fraction had a significant effect on impact force and damage area at all energies, but at higher impact levels, its effect on absorbed energy decreased because through-thickness damage mechanisms were more uniform.

The results show that hybrid laminates can be designed for specific performance, especially when the glass-basalt ratios are almost equal. While basalt-dominant laminates, with their stiffness and heat resistance, are better suited for rigid and protective structures, glass-dominant laminates are well suited for applications needing high energy absorption and flexibility, such as helmets and turbine blades. For applications requiring both toughness and stiffness, such as automotive panels, aerospace skins, and sporting goods, hybrid laminates present a promising compromise.

Limitations of the current study include the absence of microscopic failure analysis (e.g., SEM) and the exclusion of repeated or fatigue impact scenarios. To gain a better understanding of long-term performance, future studies should include fractographic analysis, cyclic loading, and microstructural characterization. Furthermore, examining the impact of fiber orientation and stacking order may help improve the hybrid response for advanced engineering applications.

Acknowledgements

The authors sincerely acknowledge Marwadi University, Rajkot, Gujarat, India, for providing financial assistance to carry out this research work.

Conflict of Interest Statement

The authors declare that they have no conflict of interest regarding the publication of this manuscript.

References

[1] Kangishwar, S., Radhika, N., Sheik, A.A., Chavali, A. & Hariharan, S., 2022. A comprehensive review on polymer matrix composites: material selection, fabrication, and application. Polymer Bulletin. 80 (1), pp. 47–87. doi:10.1007/s00289-022-04087-4..

[2] Egbo, M.K., 2020. A fundamental review on composite materials and some of their applications in biomedical engineering. Journal of King Saud University - Engineering Sciences. 33 (8), pp. 557–568. doi:10.1016/j.jksues.2020.07.007.

[3] Friedrich, K. & Almajid, A.A., 2012. Manufacturing aspects of advanced polymer composites for automotive applications. Applied Composite Materials. 20 (2), pp. 107–128. doi:10.1007/s10443-012-9258-7.

[4] Sajan, S. & Selvaraj, D.P., 2021. A review on polymer matrix composite materials and their applications. Materials Today Proceedings. 47, pp. 5493–5498. doi:10.1016/j.matpr.2021.08.034

[5] G. M N and A. N. H. Rao, "A Review on Recent Applications and Future Prospectus of Hybrid Composites," *Int. J. Soft Comput. Eng.*, vol. 1, no. 6, pp. 352–355, 2012.

[6] Czech, K., Oliwa, R., Krajewski, D., Bulanda, K., Oleksy, M., Budzik, G. & Mazurkow, A., 2021. Hybrid Polymer Composites Used in the arms industry: A review. Materials. 14 (11), pp. 304. doi:10.3390/ma14113047.

[7] S. Begum, S. Fawzia, and M. S. J. Hashmi, 2020. Polymer matrix composite with natural and synthetic fibers. *Adv. Mater. Process. Technol.*, vol. 6, no. 3, pp. 547–564. doi: 10.1080/2374068X.2020.1728645

[8] Wang, B., He, B., Wang, Z., Qi, S., Zhang, D., Tian, G. & Wu, D., 2021. Enhanced impact properties of hybrid composites reinforced by carbon fiber and polyimide fiber. *Polymers*. 13 (16), pp. 2599. doi:10.3390/polym13162599.

[9] Safri, S.N.A., Sultan, M.T.H., Jawaid, M. & Jayakrishna, K., 2017. Impact behaviour of hybrid composites for structural applications: A review. Composites Part B Engineering. 133, pp. 112–121. doi:10.1016/j.compositesb.2017.09.008

[10] Tavadi, A.R., Naik, Y., Kumaresan, K., Jamadar, N.I. & Rajaravi, C., 2022b. Basalt fiber and its composite manufacturing and applications: An overview. International Journal of Engineering Science and Technology. 13 (4), pp. 50–56. doi:10.4314/ijest.v13i4.6.

[11] Jamshaid, H. & Mishra, R., 2015. A green material from rock: basalt fiber – a review. Journal of the Textile Institute. 107 (7), pp. 923–937. doi:10.1080/00405000.2015.1071940.

[12] Dhand, V., Mittal, G., Rhee, K.Y., Park, S.-J. & Hui, D., 2014. A short review on basalt fiber reinforced polymer composites. Composites Part B Engineering. 73, pp. 166–180. doi:10.1016/j.compositesb.2014.12.011.

[13] Belingardi, G. & Vadori, R., 2002. Low velocity impact tests of laminate glass-fiber-epoxy matrix composite material plates. International Journal of Impact Engineering. 27 (2), pp. 213–229. doi:10.1016/s0734-743x(01)00040-9..

[14] Brooks, R.A., Liu, J., Hall, Z.E.C., Joesbury, A.M., Harper, L.T., Liu, H., Kinloch, A.J. & Dear, J.P., 2024. The Relationship Between the Extent of Indentation and Impact Damage in Carbon-Fibre Reinforced-Plastic Composites after a Low-Velocity Impact. Applied Composite Materials. doi:10.1007/s10443-024-10223-2.

[15] Maier, R. & Mandoc, A.-C., 2023. Investigation on layer hybridization of Glass/Carbon fibre woven reinforced composites subjected to Low-Speed Impact. Journal of Composites Science. 7 (2), pp. 83. doi:10.3390/jcs7020083.

[16] Shah, A.U.M., Sultan, M.T.H. & Safri, S.N.A., 2020. Experimental evaluation of low velocity impact properties and damage progression on Bamboo/Glass hybrid composites subjected to different impact energy levels. Polymers. 12 (6), pp. 1288. doi:10.3390/polym12061288.

[17] Ali, H.T., Akrami, R., Fotouhi, S., Pashmforoush, F., Fragassa, C. & Fotouhi, M., 2020b. Effect of the stacking sequence on the impact response of crabon-glass/epoxy hybrid composites. Facta Universitatis Series Mechanical Engineering. 18 (1), pp. 069. doi:10.22190/fume191119010a.

[18] L. Onal, L. & Adanur, S., 2002. Effect of Stacking Sequence on the Mechanical Properties of Glass–Carbon Hybrid Composites before and after Impact. Journal of Industrial Textiles. 31 (4), pp. 255–271. doi:10.1106/152808302028713.

[19] Albayrak, M., Kaman, M.O. & Bozkurt, I., 2023. The effect of lamina configuration on low-velocity impact behaviour for glass fiber/rubber curved composites. Journal of Composite Materials. 57 (11), pp. 1875–1908. doi:10.1177/00219983231164950.

[20] Santos, M., Santos, J., Reis, P. & Amaro, A., 2021. Ultrasonic C-scan techniques for the evaluation of impact damage in CFRP. Materials Testing. 63 (2), pp. 131–137. doi:10.1515/mt-2020-0020.

[21] Zhang, H., Sfarra, S. & Osman, A., 2018. Nondestructive evaluation of low-velocity impact-induced damage in basalt-carbon hybrid composite laminates using eddy current-pulsed thermography. Optical Engineering. 58 (04), 1. doi:10.1117/1.oe.58.4.041602.

[22] Zou, X., Gao, W. & Liu, G., 2023. Low-Velocity impact damage detection in CFRP laminates based on Ultrasonic Phased-Array NDT technique. Russian Journal of Nondestructive Testing. 59 (8), pp. 876–885. doi:10.1134/s1061830923600387.

[23] Shi, Y., Pinna, C. & Soutis, C., 2020. Impact Damage Characteristics of Carbon Fibre Metal Laminates: Experiments and Simulation. Applied Composite Materials. 27 (5), pp. 511–531. doi:10.1007/s10443-020-09800-y.

[24] Vescovini, A., Cruz, J.A., Ma, D., Colombo, C., Salerno, A., Bianchi, O., Amico, S.C. & Manes, A., 2023. Experimental investigation on low-velocity impact behavior of glass, Kevlar, and hybrid composites with an elastomeric polyurethane matrix. Composites Part C Open Access. 13, pp. 100426. doi:10.1016/j.jcomc.2023.100426.

[25] Ma, B., Cao, X., Feng, Y., Song, Y., Yang, F., Li, Y., Zhang, D., Wang, Y. & He, Y., 2023b. A comparative study on the low velocity impact behavior of UD, woven, and hybrid UD/woven FRP composite laminates. Composites Part B Engineering. 271, pp. 111133. doi:10.1016/j.compositesb.2023.111133.

[26] Seamone, A., Waas, A.M. & Davidson, P., 2022. Experimental analysis of low velocity impact on Carbon Fiber reinforced polymer (CFRP) composite panels. AIAA SCITECH 2022 Forum. doi:10.2514/6.2022-0409.

[27] Supian, A.B.M., Asyraf, M.R.M., Syamsir, A., Ma, Q., Hazrati, K.Z., Azlin, M.N.M., Ali, M.M., Ghani, A., Hua, L.S., SaifulAzry, S., Razman, M.R., Ramli, Z., Nurazzi, N.M., Norrrahim, M.N.F. & Thiagamani, S.M.K., 2024. Kenaf/glass fiber-

reinforced polymer composites: Pioneering sustainable materials with enhanced mechanical and tribological properties. Polymer Composites. 45 (16), pp. 14421–14447. doi:10.1002/pc.28785.

[28] Raja, D.B.P., Vettivel, S.C. & Prabhu, A.S., 2020. Influence of nanoparticles on thermal, mechanical and 3D analysis of hybrid Bamboo/Glass Fibre-Reinforced polymer composites. Transactions of the Indian Institute of Metals. 74 (1), pp. 179–193. doi:10.1007/s12666-020-02111-7.

[29] Oliveira, M., Neves, V. & Banea, M.D., 2024. Mechanical and thermal characterization of bamboo and interlaminar hybrid Bamboo/Synthetic Fibre-Reinforced epoxy composites. Materials. 17 (8), pp. 1777. doi:10.3390/ma17081777.

[30] S. D. Salman, Z. Leman, M. T. H. Sultan, M. R. Ishak, and F. Cardona, 2015. Kenaf/Synthetic and Kevlar®/Cellulosic Fiber-Reinforced Hybrid Composites: A Review. *BioResources*, vol. 10, no. 4, pp. 8580–8603.

[31] Nadzri, S.N.Z.A., Sultan, M.T.H., Shah, A.U.M., Safri, S.N.A. & Basri, A.A., 2020. A Review on the Kenaf/Glass Hybrid Composites with Limitations on Mechanical and Low Velocity Impact Properties. Polymers. 12 (6), pp. 1285. doi:10.3390/polym12061285.

[32] Arumugam, S., Kandasamy, J., Shah, A.U.M., Sultan, M.T.H., Safri, S.N.A., Majid, M.S.A., Basri, A.A. & Mustapha, F., 2020. Investigations on the mechanical properties of Glass Fiber/Sisal Fiber/Chitosan reinforced hybrid polymer sandwich composite scaffolds for bone fracture fixation applications. Polymers, 12 (7), pp. 1501. doi:10.3390/polym12071501.

[33] Vyas, C. J. and Jhala, R. L., 2024. Mechanical Characterization of Glass-Basalt Hybrid Composites with Different Fiber Weight Fraction. Mechanics of Advanced Composite Structures, 11(2), pp. 295-308

[34] D7136, A., 2012. Standard test method for measuring the damage resistance of a fiber-reinforced polymer matrix composite to a drop-weight impact event. *Annu. B. ASTM Stand.*, vol. i, no. C, pp. 1–16.

[35] Fediuk, R., Makarova, N., Qader, D.N., Kozin, A., Amran, M., Petropavlovskaya, V., Novichenkova, T., Sulman, M. & Petropavlovskii, K., 2023b. Combined effect on properties and durability performance of nanomodified basalt fiber blended with bottom ash-based cement concrete: ANOVA evaluation. Journal of Materials Research and Technology, 23, pp. 2642–2657. doi:10.1016/j.jmrt.2023.01.179.

[36] Petríková, I., Marvalová, B. & Lampa, J., 2019. Mechanical Properties of Composites with Geopolymer Matrices Reinforced by Basalt Fabric. Applied Mechanics and Materials, 889, pp. 289–293. doi:10.4028/www.scientific.net/amm.889.289.

[37] Elmahdy, A. & Verleysen, P., 2020. Comparison between the mechanical behavior of woven basalt and glass epoxy composites at high strain rates. Materials Today Proceedings, 34, pp. 171–175. doi:10.1016/j.matpr.2020.02.284.

[38] Deák, T. & Czigány, T., 2009. Chemical composition and mechanical properties of basalt and glass fibers: A comparison. Textile Research Journal, 79 (7), pp. 645–651. doi:10.1177/0040517508095597.

[39] Cai, X.J., Qin, S., An, Q.L., Zhang, H.Z., Han, S. & Chen, M., 2013. Experimental analysis on delamination damage by acoustic emission in high speed drilling of carbon fiber reinforced plastics. Key Engineering Materials, 589–590, pp. 287–292. doi:10.4028/www.scientific.net/kem.589-590.287.

[40] Zhou, Z., Sun, G., Chen, X. & Wang, J., 2014b. Detection of drilling-induced delamination in aeronautical composites by noncontact laser ultrasonic method, Applied Optics. 53 (12), pp. 2656. doi:10.1364/ao.53.002656.

[41] Goswami, M., Ghosh, M. M., Dalmiya, M. S., Sharma, S., Ghorai, S. K., & Chattopadhyay, S., 2020. A finite element method based comparative fracture assessment of carbon black and silica filled elastomers: Reinforcing efficacy of carbonaceous fillers in flexible composites. Polymer Testing, 91, Article 106856. doi:10.1016/j.polymertesting.2020.106856

[42] Quaresimin, M., Ricotta, M., Martello, L. & Mian, S., 2012. Energy absorption in composite laminates under impact loading. Composites Part B Engineering, 44 (1), pp. 133–140. doi:10.1016/j.compositesb.2012.06.020.